Temperature and Pressure Perturbations within Convective Clouds Derived from Detailed Air Motion Information: Preliminary Testing

CARL E. HANE

National Severe Storms Laboratory, Norman, Okla. 73069

BRYAN C. SCOTT

Battelle-Northwest Laboratory, Richland, Wash. 99352

(Manuscript received 26 October 1977, in final form 16 February 1978)

ABSTRACT

A method is presented for obtaining temperature and pressure perturbations within convective clouds using detailed in-cloud motion data as input. Initial testing of the iterative method indicates that it converges to a solution consistent with the input motion field. Potential applications of the method are discussed.

1. Introduction

The purpose of this article is to outline a procedure for obtaining temperature and pressure perturbation fields within convective clouds based on detailed knowledge of the motion and liquid water fields. Ultimately, it is hoped that in some cases sufficiently accurate data will be provided by multiple-Doppler radar within the clouds in combination with other measurement systems in the environment. Acquiring such data in a form compatible with the outlined analysis method is a major undertaking in itself. For this reason and because some verification is necessary to show that the method produces the "correct" result, output from a numerical model has been used as input to the analysis method in several test cases. In the following, the procedure is outlined, results of preliminary testing are reported, and a number of problems are discussed which must be overcome prior to application of the method in several possible areas.

2. The method

The basic approach involves use of the equations of motion in a form appropriate for depicting cloud scale processes. In the two-dimensional case the component equations (x,z) may be written

$$\frac{\partial u}{\partial t}+\mathbf{V}\cdot\nabla u=-\frac{1}{\rho_e}\frac{\partial p'}{\partial x}+F_x, \tag{1}$$

$$\frac{\partial w}{\partial t}+\mathbf{V}\cdot\nabla w=-\frac{1}{\rho_e}\frac{\partial p'}{\partial z}+g\left[\frac{T_v'}{T_{ve}}-\frac{p'}{p_e}-L\right]+F_z, \tag{2}$$

where in this particular application F_x and F_z have the form

$$F_x=\nu\frac{\partial^2 u}{\partial x^2}+c_m\left|\frac{\partial w}{\partial x}\right|(u_e-u),$$

$$F_z=\nu\frac{\partial^2 w}{\partial z^2}+c_m\left|\frac{\partial w}{\partial x}\right|(w_e-w),$$

and $\mathbf{V}=u\hat{\mathbf{i}}+w\hat{\mathbf{k}}$. The variables u and w are the air motion components in Cartesian coordinates (x,z), p is pressure, ρ air density, T_v virtual temperature, L the mixing ratio of condensed water, g the acceleration of gravity, ν the nonlinear viscosity coefficient, c_m a turbulent mixing coefficient and u_e and w_e height-varying horizontal and vertical wind speeds characteristic of the environment. The standard perturbation notation is used where $A=A_e+A'$, A_e being a reference value characteristic of the environment (hydrostatic in this case) and A' the deviation of A from that reference value. The viscosity coefficient ν varies in x and z according to

$$\nu=0.91(\Delta)^3\left[\left(\frac{\partial\eta}{\partial x}\right)^2+\left(\frac{\partial\eta}{\partial z}\right)^2\right]^{\frac{1}{2}},$$

where Δ is the grid distance. To simplify the forms of the equations and boundary conditions, Eqs. (1) and (2) are transformed as in Schlesinger (1975) to become

$$\rho_e\frac{\partial u}{\partial t}+\nabla\cdot\rho_e u\mathbf{V}=-p_e\frac{\partial p^*}{\partial x}+\rho_e F_x, \tag{3}$$

$$\rho_e\frac{\partial w}{\partial t}+\nabla\cdot\rho_e w\mathbf{V}=-p_e\frac{\partial p^*}{\partial z}+g\rho_e\left[\frac{T_v'}{T_{ve}}-L\right]+\rho_e F_z, \tag{4}$$

0027-0644/78/0654-0661$05.00

where $p^*=p'/p_e$ (normalized perturbation pressure), and the anelastic continuity equation has been utilized to form the terms on the left-hand side. To form a two-dimensional Poisson equation for p^*, $\partial/\partial x$ of (3) and $\partial/\partial z$ of (4) are taken and the result summed to yield

$$\nabla^2 p^* = g\frac{\partial}{\partial z}\left[\frac{\rho_e}{p_e}\frac{T_v'}{T_{ve}}\right]+G, \tag{5}$$

where

$$G=-\frac{\partial}{\partial x}\left[\frac{\rho_e}{p_e}\frac{\partial u}{\partial t}+\frac{1}{p_e}\nabla\cdot\rho_e u\mathbf{V}\right]-\frac{\partial}{\partial z}\left[\frac{\rho_e}{p_e}\frac{\partial w}{\partial t}+\frac{1}{p_e}\nabla\cdot\rho_e w\mathbf{V}\right]$$
$$-g\frac{\partial}{\partial z}\left[\frac{\rho_e L}{p_e}\right]+\frac{\partial}{\partial x}\left[\frac{\rho_e}{p_e}F_x\right]+\frac{\partial}{\partial z}\left[\frac{\rho_e}{p_e}F_z\right].$$

Eqs. (4) and (5) contain two unknowns—the perturbation pressure and the perturbation virtual temperature. To find a solution for T_v', however, the value of p^* itself is not required, only the x and z gradients of p^*. It turns out that the solution to the equations shown is not necessarily unique (as was suggested by the reviewers and verified by the authors' experimentation). To enable a unique solution to be obtained, the horizontally averaged forms of (3), (4) and (5) are subtracted from the original equations, yielding equations for $T_v'-\overline{T_v'}$ and $p^*-\overline{p^*}$, rather than T_v' and p^* [where the bar symbol denotes horizontal (x) averaging].

An iterative approach is used to solve for $T_v'-\overline{T_v'}$ and $p^*-\overline{p^*}$, using the following steps:

1) An initial guess for $T_v'-\overline{T_v'}$ is made at every grid point; e.g., $T_v'-\overline{T_v'}=0$.

2) Using the available air motion and liquid water information in Eqs. (3) and (4), the normal gradients of $p^*-\overline{p^*}$ are specified at the lateral, upper and lower boundaries.

3) Using a Poisson solver, Eq. (5) is solved subject to the Neumann boundary conditions found in step 2), i.e.,

$$\nabla^2(p^*-\overline{p^*})=g\frac{\partial}{\partial z}\left[\frac{\rho_e}{p_e}\frac{T_v'-\overline{T_v'}}{T_{ve}}\right]+G-\overline{G}.$$

4) The computed vertical gradients of $p^*-\overline{p^*}$ (obtained in step 3) are used in Eq. (4) to recompute a new value of $T_v'-\overline{T_v'}$, i.e.,

$$T_v'-\overline{T_v'}=\frac{T_{ve}p_e}{g\rho_e}\frac{\partial(p^*-\overline{p^*})}{\partial z}+H-\overline{H}, \tag{6}$$

where

$$H=\frac{T_{ve}}{g\rho_e}\left[\rho_e\frac{\partial w}{\partial t}+\nabla\cdot\rho_e w\mathbf{V}\right]+T_{ve}L-\frac{T_{ve}}{g}F_z.$$

Values of $T_v'-\overline{T_v'}$ at the upper and lower boundaries are obtained independently (either by assuming that they are known or by extrapolating from the interior). When the differences between new and previous values of $T_v'-\overline{T_v'}$ are everywhere less than some predetermined values (2×10^{-3}°C in this case), the iteration stops; otherwise step 5 is performed.

5) The normal $p^*-\overline{p^*}$ gradients at the upper and lower boundary are recomputed; a new guess of $T_v'-\overline{T_v'}$ is made based upon the new and previous value {i.e., $(T_v'-\overline{T_v'})$ (new) $=(T_v'-\overline{T_v'})$ (old) $+\alpha[(T_v'-\overline{T_v'})$ (just computed) $-(T_v'-\overline{T_v'})$ (old)]}, where α is a coefficient arrived at experimentally to maximize the rate of convergence; and at step 3 a new iteration is begun.

The preceding discussion pertains to the two-dimensional case. In three dimensions, possible methods of solution are: 1) using an identical procedure to that above on successive x,z planes; 2) solving a three-dimensional Poisson equation, thereby obtaining the entire solution field in one set of iterations; or 3) considering an altogether different method of solution. The authors have recently become aware of work by others [e.g., Gal-Chen (1978)] in three dimensions which utilizes a slightly different approach.

As it is, the approach described in this paper results in virtual temperature perturbation fields rather than temperature itself. Obtaining temperature fields from virtual temperature fields will require assumptions about or measurements of the moisture present in the solution volume. In addition, the method solution is in terms of the deviation of the perturbation virtual temperature from its horizontal average. Therefore, in the case of applying the method to field measurements, these deviation results must be combined with carefully designed aircraft (or other) observations in order to estimate the virtual temperature (or temperature) field itself.

3. Preliminary testing of the method

The scheme described above was tested for convergence and accuracy by using as input data the wind components and total liquid water content (cloud-water plus rainwater) from the two-dimensional squall line model of Hane (1973). For the most part no attempt was made to use this numerical model output data in a manner which would simulate the utilization of a typical multiple-Doppler data set. For example, no data gaps were inserted outside the cloud boundaries where multiple Doppler normally provides no velocity information. However, the upper boundary was taken to correspond closely with the cloud top in the model output in order to exclude velocity information above the cloud which would not be available from Doppler observations. The

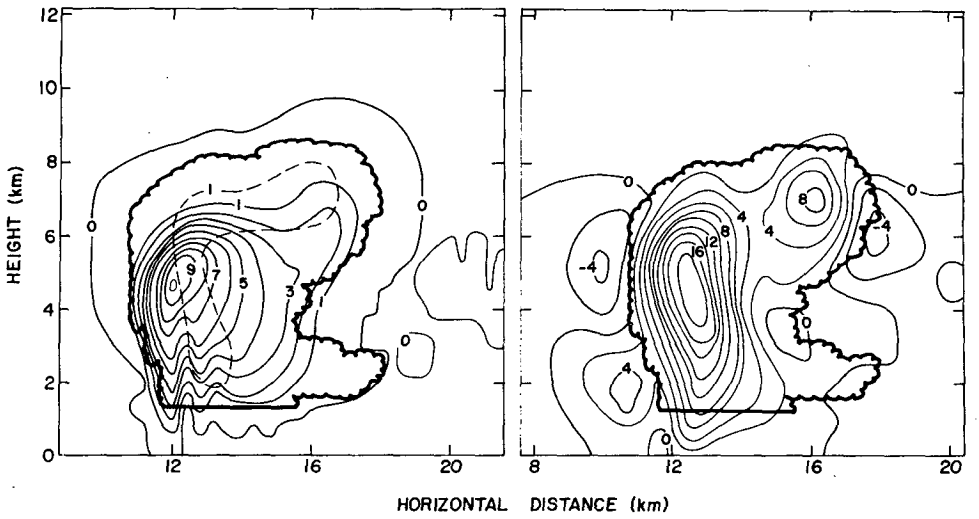

FIG. 1. Model output used as input to test the analysis method. Left: cloudwater (dashed, g kg^{-1}) and rainwater (solid, g kg^{-1}; right: vertical wind speed (m s^{-1}).

virtual temperature perturbation field produced by the method was compared with the "true" virtual temperature perturbation field obtained from the two-dimensional model.

Fig. 1 shows the cloud water, rainwater and vertical wind speed distributions output from the cloud model which were used as input to test the temperature recovery method. This particular cloud is situated in a sheared environment and is in its growth stage at this time with very little rain reaching the ground. Several unusual features are present at this time:

1) A separate area of upward flow exists in low levels to the left of the condensed cloud. This area is interpreted as a remnant of an earlier broader area of upward motion, which is being eroded by the strengthening rain-filled downdraft near the ground, and by subsidence (~5 km) compensating for the upward motion in the main upward growing updraft.

2) A secondary maximum in upward velocity (>8 m s^{-1}) is centered to the right of and slightly higher than the main updraft maximum. This appears to be bubblelike pulse being advected downwind which had its origin in low levels near the time of model initiation.

This particular time was selected because considerable detail existed in the model motion and thermal fields and it was thought that this circulation should provide a good test for the analysis method.

Fig. 2 shows the numerical model output virtual temperature anomaly for this same time. Warmest

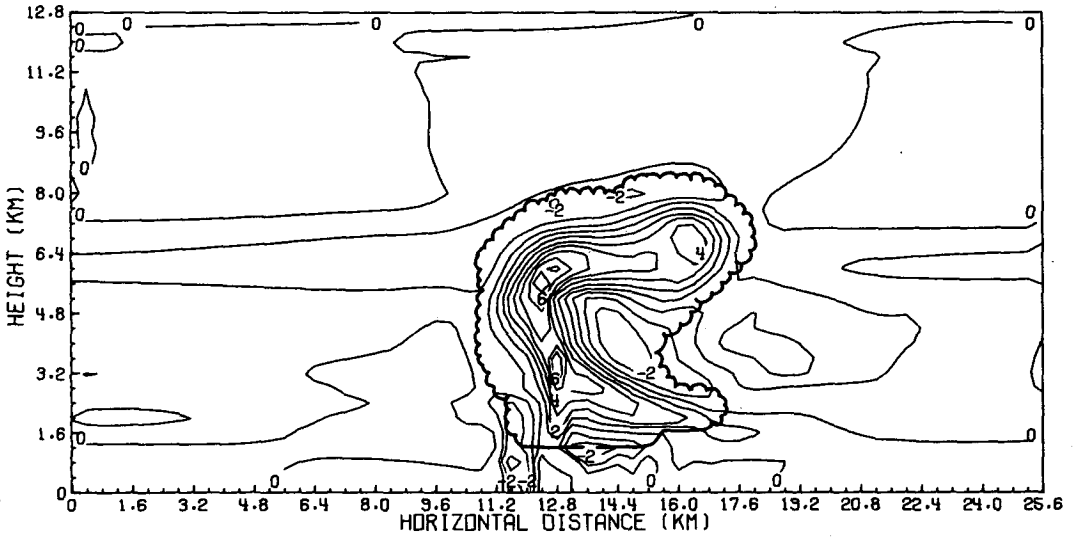

FIG. 2. Cloud model output perturbation virtual temperature deviation (°C).

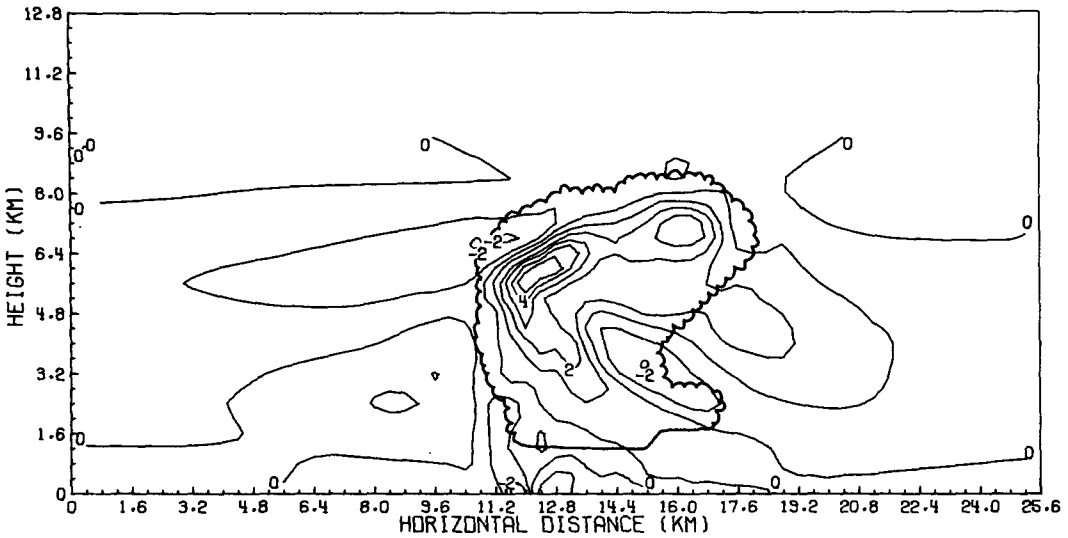

FIG. 3. Analysis method output perturbation virtual temperature deviation (°C).

temperatures within the cloud coincide with the updraft and result from the release of latent heat of condensation. Warming at least partially due to subsidence in the cloud environment is evident at 3–4 km height. Cooling at and below cloud base exists in rising slightly stable air. The cloud top is capped by cool air resulting from rising motion in stable air prior to condensation and due to evaporation of liquid water. The secondary bubble, more evident in the motion field of Fig. 1, is also present in the thermal field at 6 km in the right portion of the cloud. The cool region in the right portion of the cloud at 4 km is presumably due to evaporation of cloud by dry air incorporated from the right. Evaporation of rain has produced the cooling at the lower left-hand corner of the cloud and below.

Fig. 3 shows the virtual temperature anomaly field which was produced by the iterative analysis method. Most of the major features of the thermal field are present. Differences between model output and retrieval output are in the magnitudes of maximum values rather than in the relative locations of the important storm features. Exact agreement is not attained because the model uses a vorticity approach, whereas the retrieval method utilizes the undifferentiated momentum equations. Therefore, the finite-difference approximations for the various terms are different, leading to slightly different evaluation of

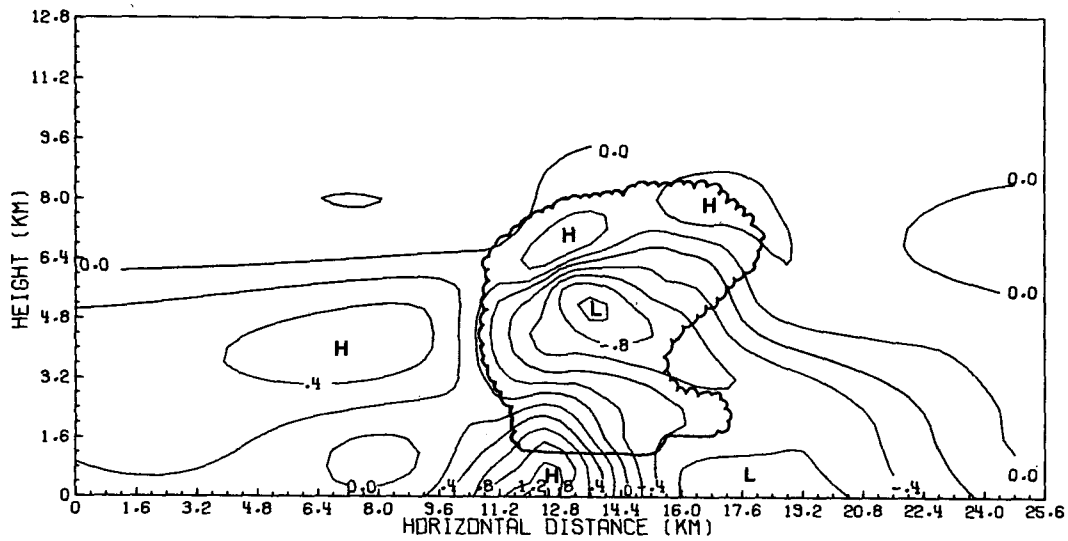

FIG. 4. Analysis method output perturbation pressure deviation (mb).

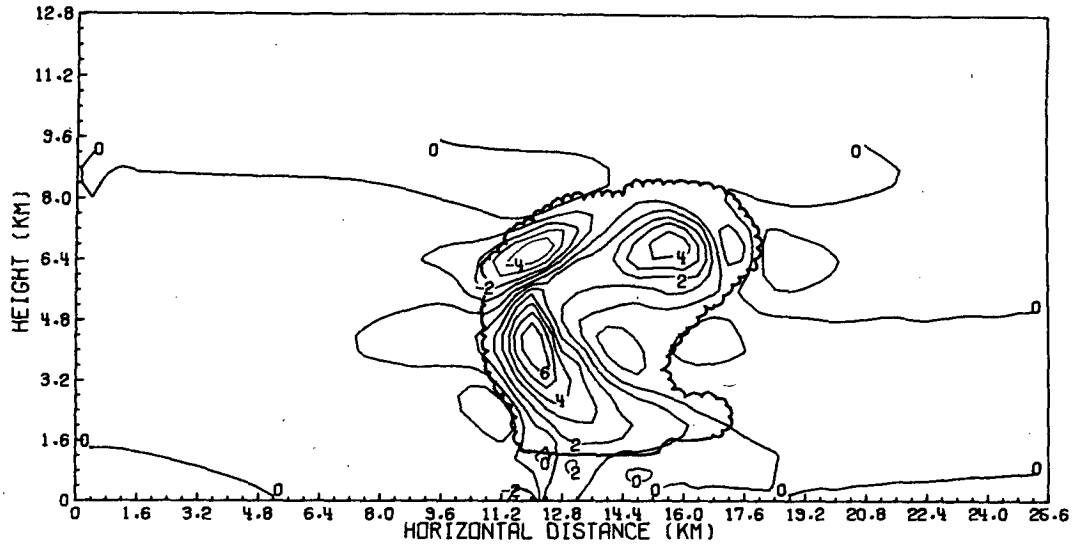

FIG. 5. Analysis method output perturbation virtual temperature deviation (°C) for case with no local time derivatives included.

terms. Additionally, the retrieval method uses a simplified version of the nonlinear viscosity term (a portion of the turbulent stress term) as compared with the model. Another difference in the physical processes is that the "pressure buoyancy" term of Eq. (2) [second term in brackets] is absent in the numerical model equations although the "perturbed pressure gradient" term [first on right in Eq. (2)] is included implicitly in the vorticity equation of the numerical model.

The maxima in the retrieval output are in almost every case lesser in magnitude than the maxima in the model output field. This suggests that perhaps an inadvertant filtering is being accomplished in the method either due to the necessary differences in the finite difference representations or in the lack of adequate representation of the turbulent stress terms in the retrieval equations. The warm anomalies in the upper portion of the updraft region are reproduced fairly well, as are 1) the warm region to the right of cloud (at ~4 km height, due to subsidence), 2) the cold regions in low levels (due to evaporation of rain) and to the right of the main updraft (4 km height) and 3) the cold cap above the cloud. Most poorly reproduced are the warm anomaly in the lower portion of the updraft and the cold pocket at cloud base.

It is expected that the agreement between model output and analysis output would be improved if the retrieval method were formulated in terms of the vorticity approach rather than the momentum approach. The results here are sufficiently good, however, to present the concept and strongly suggest that this approach is a viable one.

Because radar reflectivity data provide estimates of only the precipitation water content, the term L will often be poorly known in real data sets. To examine the influence of the condensed water mixing ratio on the final solution for T_v, a second solution was obtained by using the rainwater mixing ratio alone rather than rainwater plus cloudwater. The result was a reduction in the maximum temperature anomaly in the updraft from 5.12°C to 4.83°C (~6%). Less buoyancy was required in the updraft to achieve the given velocity distribution because of the reduction in liquid water drag. The ratio of rainwater to cloudwater in this model cloud was quite high; however, a reduction in this ratio could only be realistically achieved by decreasing the rainwater mixing ratio since the cloudwater mixing ratio seldom exceeds several grams per kilogram. But in reducing the rainwater content one is simply reducing the importance of the drag term in comparison with other terms, so that the q_r/q_c ratio ($q_r+q_c=L$) has little effect on the resulting thermal field. Errors in the absolute value of q_r are also of concern. However, it should be noted that more than 3 g kg^{-1} error in q_r is required to produce approximately 1°C error in temperature.

Also of interest is the pressure perturbation field resulting from this iterative procedure. Fig. 4 shows the field of $p'-\overline{p'}=p_e(p^*-\overline{p^*})$. The maximum magnitudes of these pressure deviations are about ±1 mb. There is a high-low couplet at the surface, consonant with the strong horizontal velocities from left to right in the "gust front" region. Low pressure is located also near the center of the cloud and high pressure near the top. Close examination of the temperature and pressure deviation fields (Figs. 3 and 4) reveals that much of the pressure field is explained hydrostatically (e.g., see the strong positive vertical gradient in pressure in the region of the maximum positive temperature deviation).

Additional solutions were obtained to ascertain the effect of omitting certain terms in the thermal retrieval equations. Fig. 5 shows the resulting temperature deviation field when the local time derivative terms are omitted. The results are not only quantitatively different, but also in some respects differ qualitatively. The largest differences (cf. Figs. 3 and 5) occur in the updraft region where the warm anomaly near the top of the updraft is partially replaced by a cold anomaly in the case with no local time change term. Also, the warming in the middle of the updraft is more pronounced in the case represented by Fig. 5. These changes are consistent with the fact that the model cloud at the analysis time contained an ascending vertical wind speed maximum which produced positive local time changes of vertical wind speed at high levels and negative changes at mid-levels. Through the third (z) component momentum equation it can be seen that inclusion of this nonsteadiness in the cloud circulation is consistent with higher positive temperature anomalies in the upper updraft and lower warm anomalies in midlevels as compared with the steady-state case.

Another experiment was performed with the local time derivative terms included again, but with the turbulent stress terms omitted. The results of this case are shown in Fig. 6, which should again be compared with Fig. 3. As expected, the magnitudes of the temperature deviations in this case are lesser than those with the turbulent stress terms included. This may be explained for the case of the updraft region, for example, by the fact that with no (basically damping) turbulent stress terms lesser thermal buoyancy is necessary to balance the input (fixed) velocity distribution.

No unique solution for temperature is possible without knowledge of the temperature at the upper and lower boundaries of the data set. That is, at the upper and lower boundaries, $\partial(p^*-\overline{p^*})/\partial z$ must be known in order to solve for $p^*-\overline{p^*}$ in the interior; therefore $T_v'-\overline{T_v'}$ must be known at each step of the iteration. If the input data are from a numerical model, there is no problem. However, in the case of Doppler-measured wind input there is no logical choice for upper boundary temperature values since the upper boundary is located near the top of the liquid water distribution rather than well above the cloud. To test the effect of various extrapolation schemes for specifying the upper boundary temperature, the upper boundary of the computational domain was lowered from 12.8 km to 9.6 km and 8.0 km in various experiments. Two extrapolation schemes were tried: 1) one simply assumes that the vertical temperature gradient does not vary with height near the upper boundary, 2) the other involves a five-point Lagrangian interpolating scheme using the temperature value at the four interior points near the boundary and the vertical gradient at the second point from the top. The vertical gradient of $T_v'-\overline{T_v'}$ is calculated by differentiating (6) with respect to height. The first method was found to give "better" answers based on comparison with the model output temperature at the upper boundary. Also, in general, the accuracy of the values of $T_v'-\overline{T_v'}$ at the first few grid points near the upper boundary appears to deteriorate the farther the boundary is lowered, although the interior values of $T_v'-\overline{T_v'}$ appeared virtually unaffected by the height of the upper boundary in relation to the cloud-top height. If future experimentation reveals that the extrapolation technique is unsatisfactory for the upper boundary condition on $T_v'-\overline{T_v'}$, then this quantity

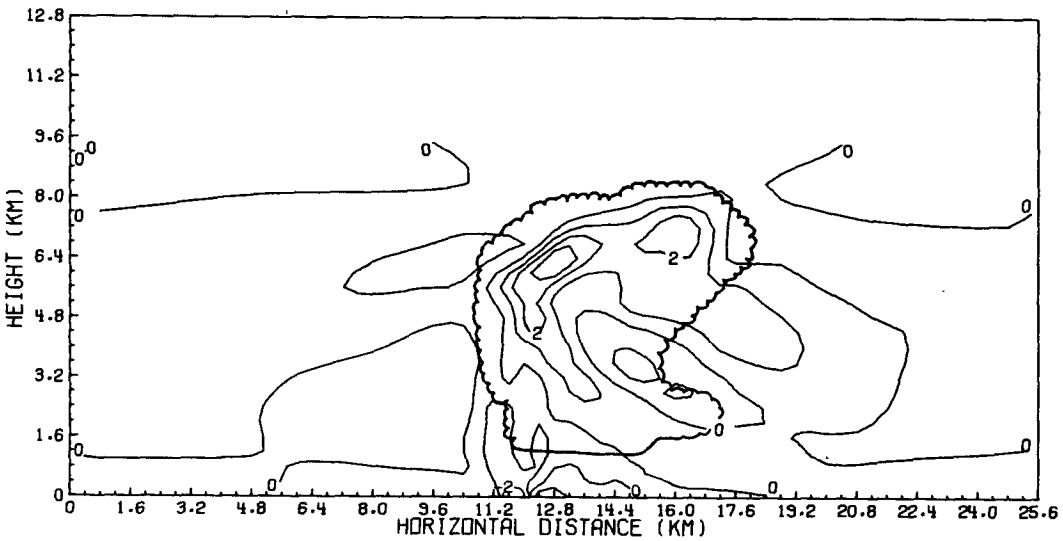

FIG. 6. Analysis method output perturbation virtual temperature deviation (°C) for case with no turbulent stress terms included.

must be based on measurements. An additional problem here is that thermal observations will probably not be available with that resolution consistent with the radar data resolution. Therefore, additional experimentation will be necessary to ascertain the sensitivity of the solution to the resolution available in $T_v'-\overline{T_v'}$ at the upper boundary.

4. Applications of the method, problems and future work

The method described was originally formulated to help deal with the hail growth-hail trajectory problem in thunderstorms observed by multiple-Doppler radar. The need to closely examine ice particle trajectories from the nucleation stage to the hail embryo stage is quite apparent. Present hail suppression techniques seek to inhibit the growth of hailstones and/or embryos by seeding in the growth regions of storms. Recirculation has been postulated in the past to be an important factor in the growth process; however, recent evidence suggests that in at least some cases simpler trajectories are indicated (Knight *et al.*, 1975). In addition, observation of hailstorms in Colorado indicate that trajectories for multicell storms (Browning *et al.*, 1976) appear significantly different than those of supercell storms (Browning and Foote, 1976). Multiple-Doppler radar observations in combination with other data may enable the calculation of ice particle trajectories and the growth of the ice particles provided that the cloud water content and the cloud temperatures can be specified. The cloud water content must be known to compute the riming (accretion) rates. The cloud temperature is required for computing the ice particle surface temperature which determines in part the riming density (and therefore the dimensions and fall velocity) and whether or not the particles experience wet or dry growth. Unfortunately, there is no direct way to measure either the cloud water content or the temperature in the entire cloud volume. One application of the method described above is to provide an indirect method for computing cloud temperature given the wind components in a three-dimensional cloud volume.

A second potential application lies in the initialization of numerical cloud models. Often a motion field is specified by the modeler as a part of the initial state and a perturbation virtual temperature field is either specified independently or does not exist. The method described here could be used, given that specified motion field, to calculate compatible virtual temperature and perturbation pressure fields and thereby avoid the possibility of initiating spurious gravity waves and a generally unrepresentative solution at times near the initial time. Such a procedure is analogous to methods used in synoptic-scale and planetary-scale modeling where in the initialization relations simpler than the time-dependent model equations are used to specify one field variable given another (e.g., geopotential from wind data).

A third potential application is very closely related to the second (and the first, for that matter). A long range goal of some cloud modelers is to take a set of observations (say, cumulus congestus data) and use it as input to a cloud model, integrate the model equations forward in time, and finally to compare their model output at a later time with another set of observations (say in the severe storm stage). The most likely observed variables to be available are the air motion components and some measure of the liquid water field within the cloud along with temperature, water vapor and horizontal wind in the environment. Therefore, to initialize a convective cloud model in the cumulus congestus stage the major remaining variables needed are the temperature, pressure, water vapor and cloudwater fields within the clouds along with all variables in transition regions between the areas of in-cloud velocity observations and environmental observations. The described method has potential use in providing several of these quantities both for initialization purposes and for verification at later observation times.

There are several problems inherent in both the first and third applications. A paramount question relates to the noise level or unrepresentative scales in the velocity fields derived from Doppler radar. This is especially important because second derivatives of velocity components are needed in the forcing function term of the $p^*-\overline{p^*}$ Poisson equation (although a reformulation of the method in terms of undifferentiated momentum equations would partially detour the problem). It may in the end be a question of whether a filtering of data sufficient to suppress unrepresentative scales permitting meaningful estimates of higher order derivatives will still allow the calculation of a meaningful thermal field. The results of thermal field calculations may indeed be used as a criterion on which to base the need and extent of future improvements in the accuracy of Doppler-derived winds. Another equally serious problem is that the method requires velocity information at every grid volume in a three-dimensional Cartesian domain, whereas velocity data will be available within irregular boundaries (e.g., see Ray *et al.*, 1975). Great effort will therefore have to be expended in order to interface the observed volume of the domain with available environmental information. Problems only slightly less serious are related to the fact that each completed scan of a storm by Doppler radar takes several minutes and storm movement coupled with nonsteady circulations within an observing interval could result in a set of observations unrepresentative of a single time. In cases where complete scans of the storm spaced closely in time are available, an updating procedure might be utilized to correct errors due to

unsteadiness. In addition, the accuracy of Doppler-derived winds is related to the forms and spatial distribution of precipitation particles. The thermal field, in turn, strongly affects the generation locations and growth mechanisms of these various particles. Thus it may be that a more complete knowledge of the thermal field will allow the derivation of more accurate air motions from Doppler observations.

Future work will be carried out within the context of COMPASS (Cooperative Observational and Modeling Project for the Analysis of Severe Storms) whose goals include improved understanding of storm structure and evolution through modeling and analysis of observations. Specific plans include 1) the assessment of the degree of sensitivity of the solution temperature fields to inaccuracies in the velocity field, 2) overcoming problems associated with using input data sets containing regions where little or no information is available and 3) extension of the method or a similar one with the same purpose to the three-dimensional case.

Acknowledgments. The authors wish to thank Dr. R. L. Alberty for suggested improvements in the manuscript and to Dr. P. S. Ray for insights into errors present in Doppler-derived winds. We are also grateful to T. Gal-Chen and an anonymous reviewer for suggestions relating to the non-uniqueness of the solution as the method was originally proposed. The manuscript was typed by Sandra Mudd and Connie Hall.

REFERENCES

Browning, K. A., J. C. Fankhauser, J. P. Chalon, P. J. Eccles, R. G. Strauch, F. H. Merrem, D. J. Musil, E. L. May and W. R. Sand, 1976: Structure of an evolving hailstorm. Part V: Synthesis and implications for hail growth and hail suppression. *Mon. Wea. Rev.*, **104**, 603–610.

——, and G. B. Foote, 1976: Airflow and hail growth in supercell storms and some implications for hail suppression. *Quart. J. Roy. Meteor. Soc.*, **102**, 499–533.

Gal-Chen, T., 1978: On matching three dimensional convection models with observations. Submitted to *Mon. Wea. Rev.*

Hane, C. E., 1973: The squall line thunderstorm: numerical experimentation. *J. Atmos. Sci.*, **32**, 1672–1690.

Knight, C. A., D. H. Ehhalt, N. Roper and N. C. Knight, 1975: Radial and tangential variation of deuterium in hailstones. *J. Atmos. Sci.*, **32**, 1990–2000.

Ray, P. S., R. J. Doviak, G. B. Walker, D. Sirmans, J. Carter and B. Bumgarner, 1975: Dual-Doppler observation of a tornadic storm. *J. Appl. Meteor.*, **14**, 1521–1530.

Schlesinger, R. E., 1975: A three-dimensional numerical model of an isolated deep convective cloud: preliminary results. *J. Atmos. Sci.*, **32**, 934–957.